Appl. Phys. A (2016)122:276
DOI 10.1007/s00339-016-9835-y

Applied Physics A
Materials Science & Processing

Texture analysis of Napoleonic War Era copper bolts

Florencia Malamud[1] · Shirley Northover[2] · Jon James[2] · Peter Northover[3] · Joe Kelleher[4]

Received: 19 October 2015 / Accepted: 17 February 2016

Abstract Neutron diffraction techniques are suitable for volume texture analyses due to high penetration of thermal neutrons in most materials. We have implemented a new data analysis methodology that employed the spatial resolution achievable by a time-of-flight neutron strain scanner to non-destructively determine the crystallographic texture at selected locations within a macroscopic sample. The method is based on defining the orientation distribution function of the crystallites from several incomplete pole figures, and it has been implemented on ENGIN-X, a neutron strain scanner at the Isis Facility in the UK. Here, we demonstrate the application of this new texture analysis methodology in determining the crystallographic texture at selected locations within museum quality archaeological objects up to 1 m in length. The results were verified using samples of similar, but less valuable, objects by comparing the results of applying this method with those obtained using both electron backscatter diffraction and X-ray diffraction on their cross sections.

✉ Florencia Malamud
fmalamud@cab.cnea.gov.ar

[1] Laboratorio de Física de Neutrones, Centro Atómico Bariloche, Av. Bustillo 9500, San Carlos de Bariloche, 8400 Rio Negro, Argentina

[2] Materials Engineering, The Open University, Walton Hall, Milton Keynes MK7 6AA, UK

[3] Research Laboratory for Archaeology and the History of Art, South Parks Rd, Oxford OX1 3QY, UK

[4] Rutherford Appleton Laboratory, ISIS Neutron and Muon Source, Harwell Oxford, Didcot 0X11 0QX, UK

1 Introduction

Neutron diffraction has been used as a non-destructive technique to study cultural heritage samples for several years. In particular, due to the high penetration of thermal neutrons in most materials, neutron diffraction techniques have been employed for volume texture analyses in archaeological samples: in ancient copper and copper alloy objects [2, 14, 15], Renaissance bronze statuettes [16] or sixteenth-century silver coins [15]. Such analyses are often constrained by the complex geometry of the objects and by the inherent inhomogeneity of archaeological and historic materials. In this context, spatially resolved neutron texture analyses offer a great advantage, as small parts of a museum piece could be analysed separately, allowing the identification of material properties and the manufacturing routes of the individual components. Recently, this idea was implemented in Ref. [9] using ENGIN-X [13] a time-of-flight (TOF) neutron strain scanner, which allows diffraction measurements to be made deep within the samples. In standard strain scanning experiments, all neutrons arriving at a detection bank are *time-focussed* into a single diffractogram by a post-analysis routine. The texture analysis method is based on splitting the relatively large solid angle covered by ENGIN-X detection banks into smaller detection units ("virtual detectors"), to improve the angular resolution and increase the number of directions explored for a fixed orientation of the specimen. The method defined the orientation distribution function (ODF) of the material from a number of incomplete experimental pole figures using the MTEX Toolbox [6]. The best estimate of the ODF is computed as the solution of a minimization problem, based on a model regarding the diffraction counts as deriving from a Poisson process.

This paper demonstrates the application of this new texture analysis methodology in determining, non-

Published online: 07 March 2016

destructively, the crystallographic texture at selected locations within archaeological objects up to 1 m in length. The results are verified using samples of similar but less valuable objects by comparing the results of applying this method with those obtained using both electron backscatter diffraction (EBSD) and X-ray diffraction (XRD) on their cross sections.

2 Samples

When the warships of the British Royal Navy were first experimentally sheathed in copper to protect them against shipworm and fouling, problems very quickly became apparent. The planks and frames of the ships were fastened with iron bolts, and electrolytic action between the copper and iron in seawater led to severe degradation of the iron. In time the advantages of coppering the ships were seen to be so extensive that an answer had to be found. Two main approaches were tried: for smaller ships up to 50 guns forged copper bolts were used, but there was clearly doubt about their suitability for the largest ships of up to 100 guns. Instead expedients such as lacquering the copper or putting a layer of paper and preparations with a variety of compositions between the copper and the iron were tried, but found to be of limited use. Alloy bolts were also experimented with, but finally it was decided to use cold-rolled copper bolts, for which three patents were taken out in 1783. Two of these patents, those of William Forbes and John Westwood, used grooved rolls to achieve the desired diameters, while the third, by William Collins, used grooved rolls to draw the copper bar through a die. The copper used by each was of very similar composition and quality, but it should, in theory, have been possible to identify the products of each manufacturer because each was supposed to stamp the bolts with their name. However, this did not happen.

The bolts recovered during the excavation of a shipwreck have an important part to play in both identifying the ship and understanding its construction and history. The characterization of bolts from two identified wrecks, *HMS Pomone*, completed in 1805 and lost in 1811 and *HMS Impregnable*, completed in 1786 and lost in 1799, led to the application of texture analysis by neutron diffraction described in this paper. Initially, EBSD was used to examine the deformation of the copper during the manufacture and use of the bolts, because conventional optical metallography was not always successful in revealing deformation structures. In the course of this, a bolt from the *Pomone* was found to have a strong fibre texture, which linked it to William Collins' patent. The question then arose of determining the texture of bolts produced by the other processes. In one case, this was straightforward, because a bolt with a Forbes stamp on it was recovered from the *Impregnable*. Documentary evidence shows that Forbes' rolling mill was ready for use on 23 October 1783 and in November he received an order for bolts for the *Impregnable*. At that time, he was the only patentee with a working rolling mill and a Navy contract. The bolt (Fig. 1) is of museum quality, which precluded removal of a cross section for texture analysis by EBSD or XRD, but the high penetration of neutrons enabled noninvasive investigations of the texture of different regions of two complete bolts and a segment of a third, incomplete, one, which was available for subsequent sectioning and examination using EBSD and XRD.

2.1 HMS Pomone

HMS *Pomone*, a "fifth rate", 38-gun frigate of the Leda class, was laid down at Brindley's Yard on the Medway at Frindsbury in December 1803 and completed on 17 January 1805. No subsequent repairs are documented, so the bolts recovered from her wreck will be original. The complete bolt studied here finds number AB1-02-01 in the excavation archive, is a blind bolt 330 mm long and 22.5 mm in diameter and was possibly used for fastening planking to a frame. The other Pomone sample, the "bolt segment", was cut from a fragment of a bolt from HMS Pomone which had previously been used for machining tensile test specimens. The bolt was originally 33.5 mm in diameter.

2.2 HMS impregnable

HMS *Impregnable*, a "second rate", 90-gun ship of the line of the *London* Class, was laid down at HM Dockyard, Deptford in October 1780. In late 1783, it was ordered that where possible any iron bolts should be driven out and replaced with copper; copper bolts were ordered from William Forbes in November 1783 and the bolt studied here has a Forbes stamp. *Impregnable* was completed in

Fig. 1 HMS *Impregnable* bolt with a Forbes works stamp

May 1786 and had some repairs in 1794. The bolt studied here, IMP-006 in the excavation archive, is 956 mm long and 35.5 mm in diameter, is probably joined major timbers in the fore part of the ship and is probably original to her construction. The bolt is one of very few with a Forbes works stamp, as is shown in Fig. 1 (inset).

3 Texture measurements

The neutron diffraction experiments were performed on the ENGIN-X instrument, a time-of-flight (TOF) neutron diffractometer, at the ISIS Facility, Rutherford Laboratory, UK, optimized to measure the precise position of diffraction peaks from a small, well-defined volume of a bulk component. Detailed information about the instrument is given in Ref. [13], so only a brief description is provided here. A pulsed polychromatic neutron beam travels along a curved neutron guide and impacts on a bulk sample at $\sim$50 m from the source. Figure 2a shows a schematic view of ENGIN-X at the sample position, here represented by a cylinder. The neutrons scattered into a range of directions approximately perpendicular to the incident beam are collected by detection banks (the North and South banks in the figure). Each bank is composed of 1200 individual detectors, arranged in 240 columns and five rows, represented in Fig. 2a as black rectangles. The region of the object from which the instrument collects information, the "gauge volume", corresponds to the cuboid lying at the intersection of the incident and diffracted beams (represented by a small dark rectangle inside the sample). ENGIN-X also has a transmission detector aligned with the incident beam to record the unscattered neutrons as a function of their TOF. The detector is pixelated, composed of a 10 $\times$ 10 array of 2-mm cubes of scintillating glass GS20 [12].

The texture analysis strategy applied in this work is based on defining the ODF of the crystallites from several incomplete pole figures using NyRTex [9] a freely available package for texture analysis. The data analysis scheme implemented in NyRTex is based on splitting the ENGIN-X detection banks into a number of detector units. This is done by time-focussing the 1200 detection elements composing a bank into smaller groups, with each of these *virtual detectors* hence covering a smaller solid angle. As an example, in Fig. 2a each detection bank has been subdivided into ten smaller units in a 2 $\times$ 5 (horizontal $\times$ vertical) gridding scheme, and each sub-unit has been identified by a number (1–10). For this case, each virtual detector is composed by a group of 24 $\times$ 5 = 120 detectors elements, covering $\sim$8° in the vertical plane and $\sim$8° in the horizontal plane. Figure 2b shows a typical diffractogram recorded by the virtual detector labelled 3 from the "bolt segment", oriented as shown in Fig. 2a. Each diffraction peak hkl provides information about the number of crystallites having their {hkl} plane normals close to the direction of the bolt axis (BA). The ranges of directions covered by each virtual detector shown in Fig. 2a are identified in the stereogram shown in Fig. 2c. Measurements taken at several different rotations and tilts of the sample are needed to determine the complete pole figure. At ENGIN-X a choice of different goniometers are available to achieve this, depending on size and weight of the specimen being investigated.

3.1 Experimental pole figure

The construction of an experimental pole figure $P_{hkl}(\alpha, \beta)$ requires a quantitative determination of the integrated peak area recorded by a virtual detector along a certain direction of the specimen (α = latitude, β = longitude). In order to produce a combined pole figure from data registered by different virtual detectors, several corrections need to be applied to the refined peak area measured by each individual virtual detector. In addition to the (unknown) texture factor, the integrated intensity of a diffraction peak measured in a TOF diffractometer depends on the scattering power (G_{hkl}) and linear absorption coefficient (μ_{hkl}) of the sample, as well as on an instrumental factor (Φ^j_{inst}) specific to each virtual detector (j). Hence, the pole figure intensity (P_{hkl}) recorded by a virtual detector is obtained from the measured integrated peak area (I_{hkl}) according to

$$P_{hkl}(\alpha, \beta) = I_{hkl}(\alpha, \beta) / \left(G_{hkl} \exp(-l\mu_{hkl}) \Phi^j_{\text{inst}} \right) \quad (1)$$

with l being the length of the neutron path inside the specimen.

3.1.1 Integrated peak areas

The integrated areas of selected peaks of the diffractograms are obtained by least-squares fitting to the experimental data, using a multi-peak fitting algorithm based on asymmetric peak profiles (each the convolution of a Gaussian with a truncated exponential [8]) superimposed on a linear background.

3.1.2 Scattering power

The scattering power is given by $G_{hkl} = \frac{m_{hkl} |F^2_{hkl}| d^4_{hkl}}{v_0^2}$ where v_0 is the volume per atom, F^2_{hkl} the structure factor (including the Debye–Waller factor), m_{hkl} the multiplicity of the reflection and d_{hkl} the interplanar distance of the particular reflection.

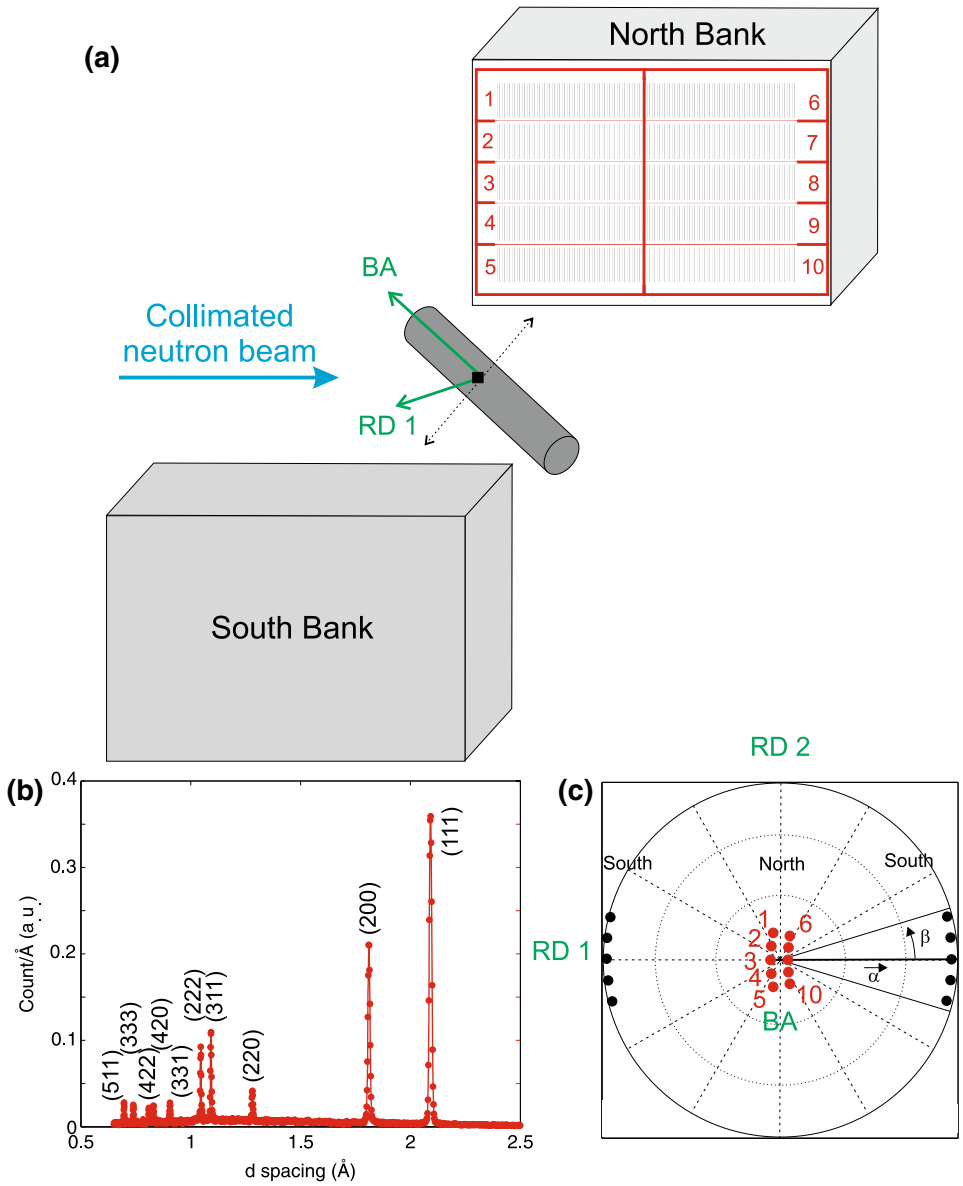

Fig. 2 **a** Schematic diagram of the ENGIN-X time-of-flight neutron strain scanner, with a bolt (*cylinder*) at the sample position. Each detection bank has been subdivided into ten virtual detectors in a 2 × 5 (horizontal × vertical) gridding scheme. The virtual detectors have been identified by a number (1–10) at North Bank. **b** Typical diffractogram recorded from the "bolt segment" using the virtual detector labelled 3. **c** Stereogram showing the approximate angular coverage and locations of the virtual detectors, and the angular convention adopted in constructing the experimental pole figures

3.1.3 *Instrumental factor*

The instrumental factor is given by

$$\Phi^{j}_{\text{inst}} = \Phi^{j}_{0}(\lambda)\varepsilon_j(\lambda)\frac{h_j}{\pi L_j}\alpha^{\text{vert}}_{\text{in}}\sin^2\theta_{B,j}\left[\left(\alpha^{\text{hor}}_{\text{in}}\right)^2+\left(\alpha^{\text{hor}}_{j}\right)^2\right]^{1/2}\delta V \quad (2)$$

where $\theta_{B,j}$, L_j and h_j are, respectively, the mean Bragg angle, distance to sample and height of the j virtual detector; $\Phi^{j}_{0}(\lambda)$ and $\varepsilon_j(\lambda)$ are, respectively, the incident neutron flux and detection efficiency at the wavelength $\lambda = 2d_{hkl}\sin\theta_{B,j}$; δV is the gauge volume, i.e., the volume of the sample illuminated by the neutron beam that is effectively seen by the detector; $\alpha^{\text{hor}}_{\text{in}}$ and $\alpha^{\text{vert}}_{\text{in}}$, are the divergences of the incident beam in the diffraction plane and normal to it, respectively; and α^{hor}_{j} is the divergence of the scattered beam seen by the detector, as allowed by the radial collimator. The wavelength dependence of Φ^{j}_{inst} is contained in the product term Φ^{j}_{0} (λ) ε_j (λ), usually approximated by measuring the spectra scattered by a V3%Nb sample (which is assumed to be a perfectly elastic-incoherent scatterer) under the same experimental conditions.

3.1.4 *The linear absorption coefficient*

The material attenuation coefficient is given by: $\mu = N\sigma_{\text{tot}}$, with N being the number of atoms per unit volume and σ_{tot} the material's microscopic total cross section. The total cross section of polycrystalline materials has a complex

dependence on neutron wavelength; however, in a first approximation, it is directly related to the transmission of the specimen by,

$$\mathrm{Tr}(\lambda, \boldsymbol{\tau}) = \exp(-Nl\sigma_{\mathrm{tot}}(\lambda, \boldsymbol{\tau})) \quad (3)$$

where $\boldsymbol{\tau}$ indicates the direction of the transmitted neutron beam in the coordinate system of the sample. In this work, the total cross section for each sample was calculated from the transmission spectrum measured with the bolt axis vertical. The dotted green line in Fig. 3a is the total cross section expected for a powder sample, while the blue crosses are experimental values measured for the Forbes bolt with its axis vertical. The differences between the experimental results and the theoretical curve derived for a powder specimen reveal that the total cross section is highly sensitive to the crystallographic texture of the material.

Since, a diffraction peak measured on a TOF diffraction bank contains contributions from neutrons with a range of wavelengths, from $\lambda_{\min} = 2d_{hkl}\sin\theta_{\min}$ to $\lambda_{\max} = 2d_{hkl}\sin\theta_{\max}$ where $\theta_{\min}$ and $\theta_{\max}$ are the minimum and maximum Bragg angles of neutrons incident on the detector bank; the attenuation coefficient μ_{hkl} for a particular reflection can be calculated by averaging the total cross section over the associated wavelength range [17]:

$$\mu_{hkl} = \frac{N\int_{2d_{hkl}\sin\theta_{\min}}^{2d_{hkl}\sin\theta_{\max}} \sigma_{\mathrm{tot}}(\lambda)\mathrm{d}\lambda}{2d_{hkl}(\sin\theta_{\max} - \sin\theta_{\min})} \quad (4)$$

3.1.5 Neutron path *l*

For each sample orientation and for each virtual detector, the neutron path lengths inside the specimens were calculated using the virtual sample and instrument models comprising the SScanSS virtual laboratory [7].

4 Experiments

For all three samples, the neutron experiments were performed on ENGIN-X using a gauge volume of $4 \times 4 \times 4$ mm^3 and an incident beam divergence optimized for texture measurements, of $\approx 0.7° \times 0.8°$ (horizontal $\times$ vertical). To investigate the texture along different specimen directions, the samples were placed with the bolt axis horizontally (as is shown in Fig. 1a), vertically (i.e., normal to the page in Fig. 1a) and tilted to 45° from the vertical. Following the cylindrical symmetry of the samples, a macroscopic coordinate system was defined, for each bolt, by the bolt axis direction (BA) and two perpendicular radial directions (RD 1 and RD 2), arbitrarily defined. For each bolt axis configuration, several measurements were taken, rotating the sample around the vertical instrument axis using the ENGIN-X rotation stage, with counting times of $\sim$12 min per orientation. Simultaneously, for each orientation, the neutron transmission spectrum was collected using the transmission detector. It is important to keep in mind that this transmission spectrum is measured from neutrons having travelled the length of the full path of the beam through the sample. This might differ significantly from the spectrum at the gauge volume under investigation by diffraction.

The pole figure coverage achieved by this texture measurement strategy is strictly dependent on the range of orientations explored by the experiment and the gridding scheme employed to analyse the data. In general, the pole figure coverage is always incomplete and the locations of the experimental data in the pole figure define the accuracy of the resulting ODF. To test the texture analysis methodology and the pole figure coverage needed to fully describe the bolts texture, the ODFs obtained with the present method have been validated by complementary

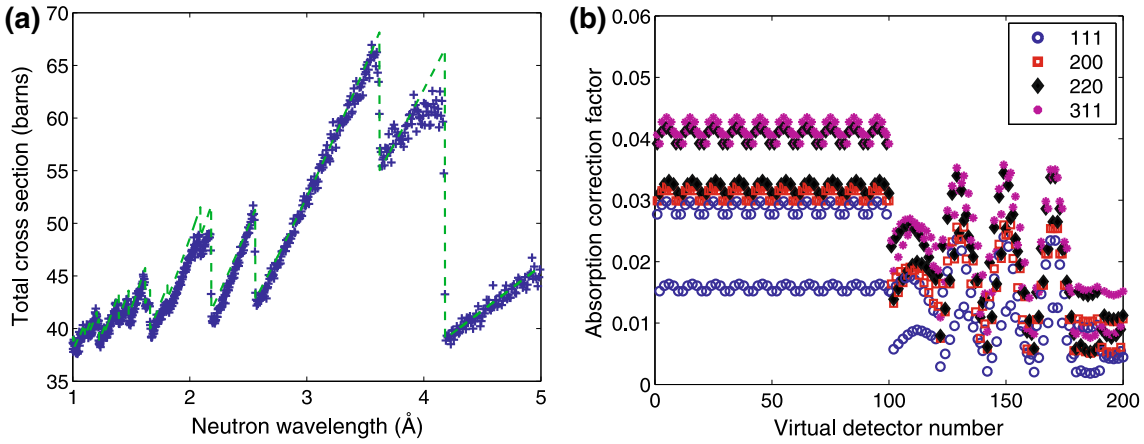

Fig. 3 **a** Experimental (*blue crosses*) neutron total cross section of the Forbes bolt sample along the radial direction RD1 and total cross section expected for a powder sample (*green dotted line*). **b** The absorption correction factors calculated for different reflections, using the individual flight paths for the virtual detectors used in the Forbes bolt experiment

experiments on the segment sample using other, more conventional, texture techniques. This included EBSD measurements and laboratory X-ray diffraction in reflection geometry.

5 Data analysis strategy

The full orientation distribution functions (ODF) have been reconstructed from the experimental data using NyRTex. In this case, the data were analysed in a 2×5 (horizontal $\times$ vertical) gridding scheme, which gives each virtual detectors coverage of $\sim 8^\circ \times 8^\circ$ in angular space. A single diffractogram was compiled for each virtual detector, by adding together the TOF spectra recorded by all the individual detector elements belonging to that group using a common d-spacing scale. This analysis strategy produces a total of 200 virtual detectors for the 10 orientations measured for each sample.

Due to the bolts' large diameters, the path lengths for some virtual detectors were ~ 0.05 m, which generates a small absorption correction factor for some reflections ($\exp(-l\mu_{hkl}) < 0.01$). Figure 3b shows the absorption correction factors for the 111, 200, 220 and 311 reflections, from the gauge volume of the Forbes bolt, incident on the different virtual detectors. With such large path lengths, the integrated peak areas recorded by the virtual detector are governed by absorption, rather than texture. Because of this high absorption, the peak fitting routine is unreliable, so the affected virtual detectors were not used in the analysis. For each sample, the {111}, {200}, {220} and {311} experimental pole figures were generated using the integrated intensities and the respective correction factors for the virtual detectors with $\exp(-l\mu_{hkl}) > 0.01$. The resulting pole figure coverage is shown in Figs. 4b, 6b and 7b for the "segment sample", AB1-02-01 sample and Forbes bolt, respectively. The ODF was calculated from the experimental pole figures with MTEX, assuming triclinic sample symmetry.

6 Texture results and interpretation

The texture results are presented as the {111}, {200} and {110} copper pole figures and by the ODF sections showing the principal texture components. Figures 4c, 5c and 6c display the pole figures reconstructed by the NyRTex analysis. For the three samples, the bolt axis direction corresponds to the centre of the pole figure. The colour scale represents pole densities in multiples of random distribution (mrd) units. Densities are normalized with respect to the average (random) distribution; thus, a one-colour pole figure showing uniform density of 1.0 mrd would indicate the absence of texture.

6.1 HSM Pomone

6.1.1 Segment sample

6.1.1.1 Neutron diffraction texture results The experimental {111} pole figure (Fig. 4b) shows the coverage achieved with the measurement strategy used for the bolt segment sample (Fig. 4a). The recalculated pole figures (Fig. 4c) show a marked double fibre texture. A better insight on texture can be gained from the $\varphi_2 = 45^\circ$ ODF cut, shown in Fig. 4d, where the main texture components are well represented. The intense band found at $\Phi = 55^\circ$ is the γ-fibre with {111} planes parallel to the bolt axis with a volume fraction of 40 % of the crystallites, and the other component (with 12.5 % of the crystallites) is a ⟨100⟩ fibre component. This double fibre texture is typical of axisymmetrically drawn products made of face-centred-cubic (fcc) metals with medium or high stacking fault energies [3], consisting of double fibres with a majority ⟨111⟩ component and a minority ⟨100⟩. This major component is one of the most common fibre textures, having the {111} slip plane perpendicular to the direction of application of the force. On the other hand, the presence of a ⟨100⟩ fibre texture reveals nearly complete thermal crystallization after working [10].

6.1.1.2 EBSD texture results After the neutron experiments, the bolt segment was cut along a cross section through the centre of the gauge volume and a sample prepared for EBSD texture measurements [11] from this area of the gauge volume. The sample was prepared by conventional mechanical methods; grinding and diamond polishing, sequentially to a 1-μm finish, before final preparation by light etching for 5–10 s in equal proportions of distilled water, concentrated ammonium hydroxide and 3 % hydrogen peroxide.

The small amount of material lost in this preparation displaced the plane of observation from the centre of the gauge volume of the neutron experiments, but the material examined by EBSD still lay well within it. EBSD was performed in a Zeiss Supra VP field emission gun scanning electron microscope fitted with a Nordlys detector. All measurements were taken at 20 kV, using the high current mode. Aztec (Oxford Instruments) software and MTEX were used for the acquisition and post-processing, respectively.

Figure 5a shows pole figures derived from EBSD measurements over an area of approximately 2 mm $\times$ 1.5 mm at the centre of a cross section through the bolt segment taken in a plane in which the neutron measurements were taken. It is immediately obvious that the two techniques have given almost identical results with the maximum preferred alignment of ⟨111⟩ along the bolt axis being

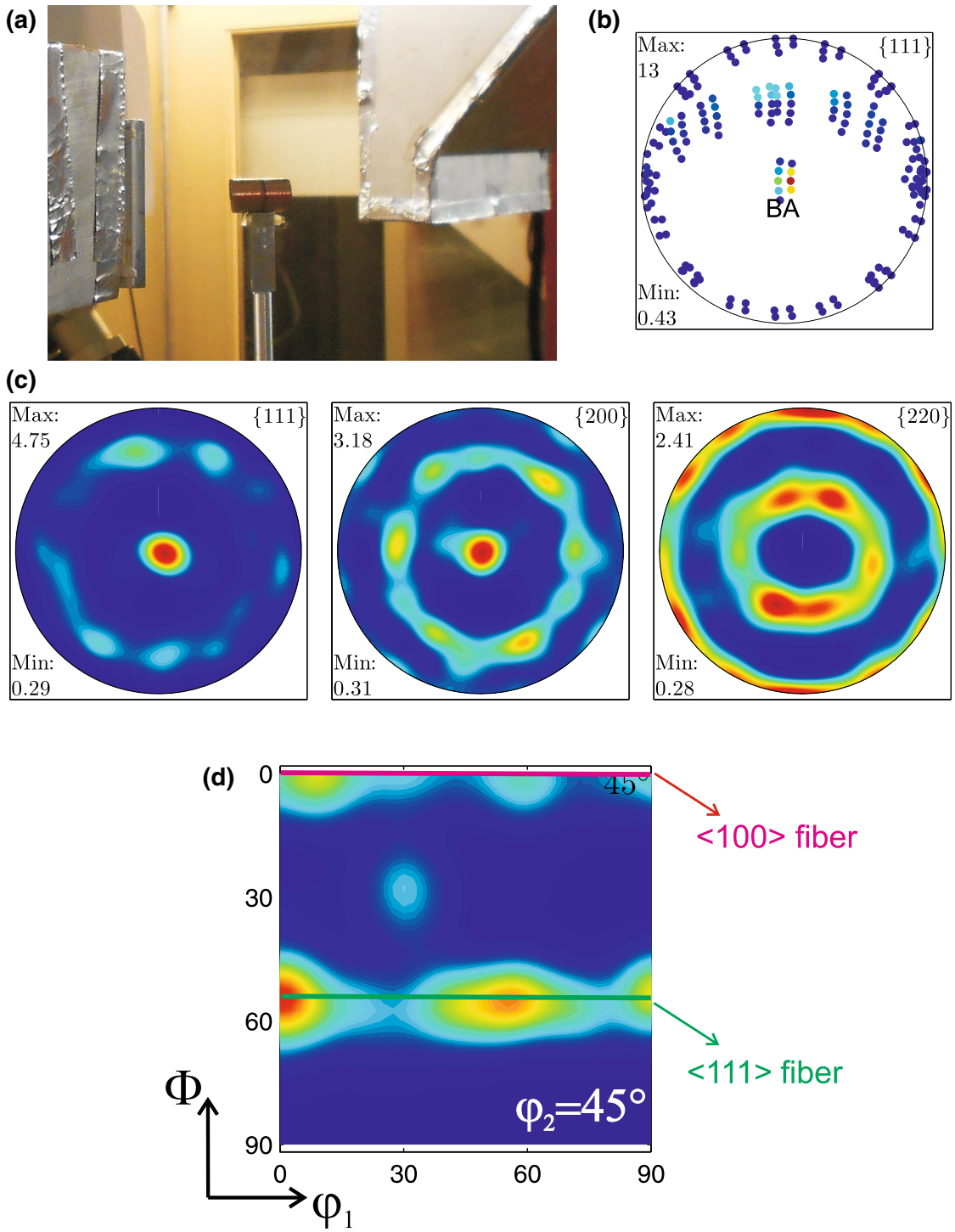

Fig. 4 **a** Photograph of the bolt segment sample in ENGIN-X. **b** The experimental pole figure showing the angular coverage achieved by the measurement. **c** Recalculated pole figures from the ODF calculated with MTEX from experimental pole figures such as (**b**). **d** Cut of the ODF at $\varphi_2 = 45°$, showing the main texture components of the material

measured as 5 by EBSD and 4.75 by the new neutron technique. The orientation image of Fig. 5b confirms the grain structure to be fully recrystallized. The variations of colour within the individual grains reflect the moderate levels of deformation in the recrystallized grains.

6.1.1.3 X-ray texture measurement The bolt segment's texture was also measured using laboratory X-ray diffraction in reflection geometry, in a Panalytical X-pert MPD diffractometer with Cu K_α radiation. The analysis was performed using MTEX software, with a prior defocusing

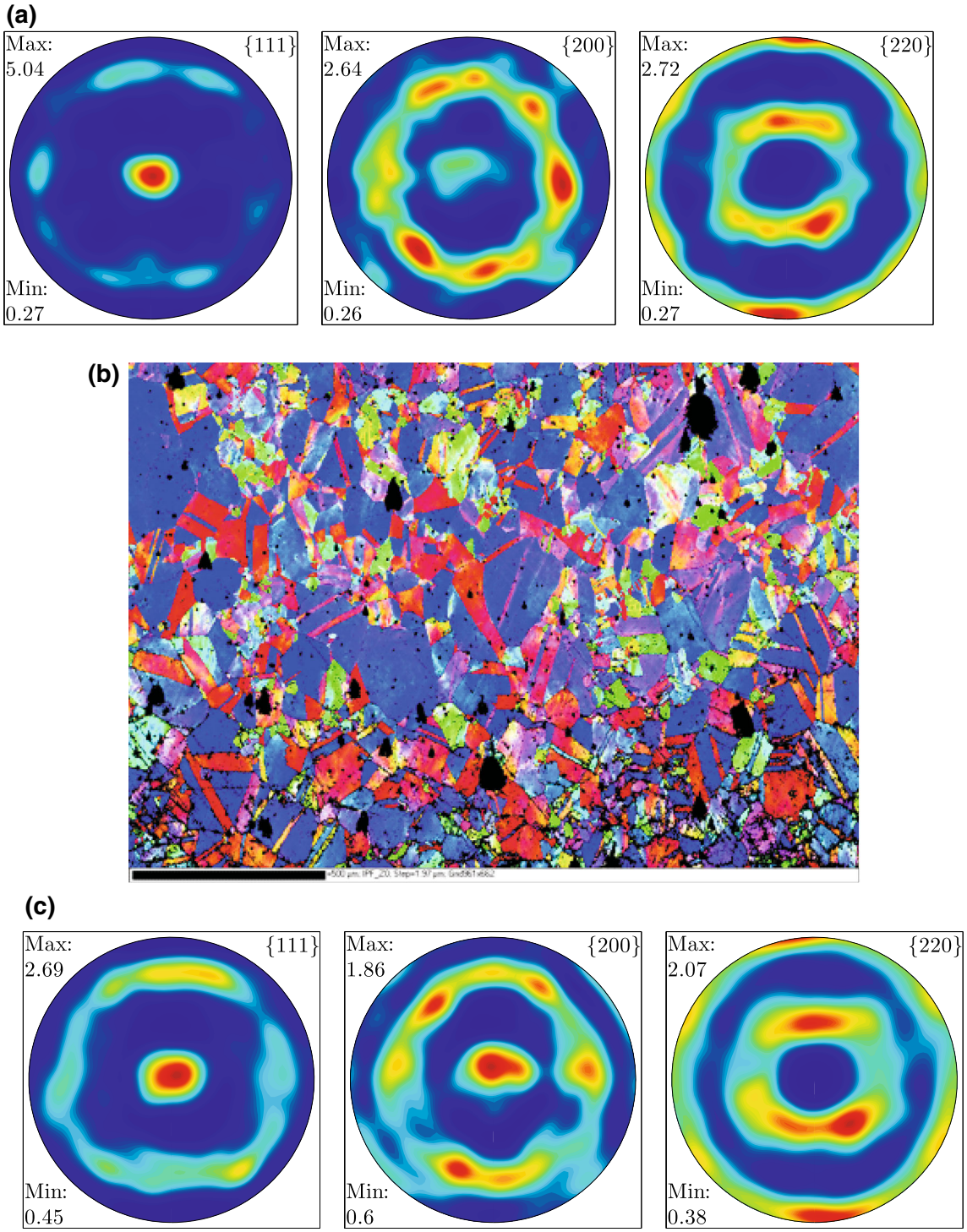

Fig. 5 **a** Pole figures derived from EBSD measurements over an area approximately 2 mm × 1.5 mm at the centre of the cross section of the bolt segment examined by TOF neutron diffraction. **b** EBSD orientation map of the same area showing fully recrystallized grain structure with deformation within the individual grains. **c** Recalculated pole figures from accompanying X-ray diffraction experiments

correction, to ensure proper calculation of consistent orientation distribution functions (ODFs) and recalculated pole figures. As is shown in Fig. 5c, the recalculated pole figure also presents a marked double fibre texture, with a strong γ-fibre and a minor $\langle 100 \rangle$ fibre component. The volume fractions obtained for each component using the different texture analysis measurements are given in Table 1. The results show the consistency of the three

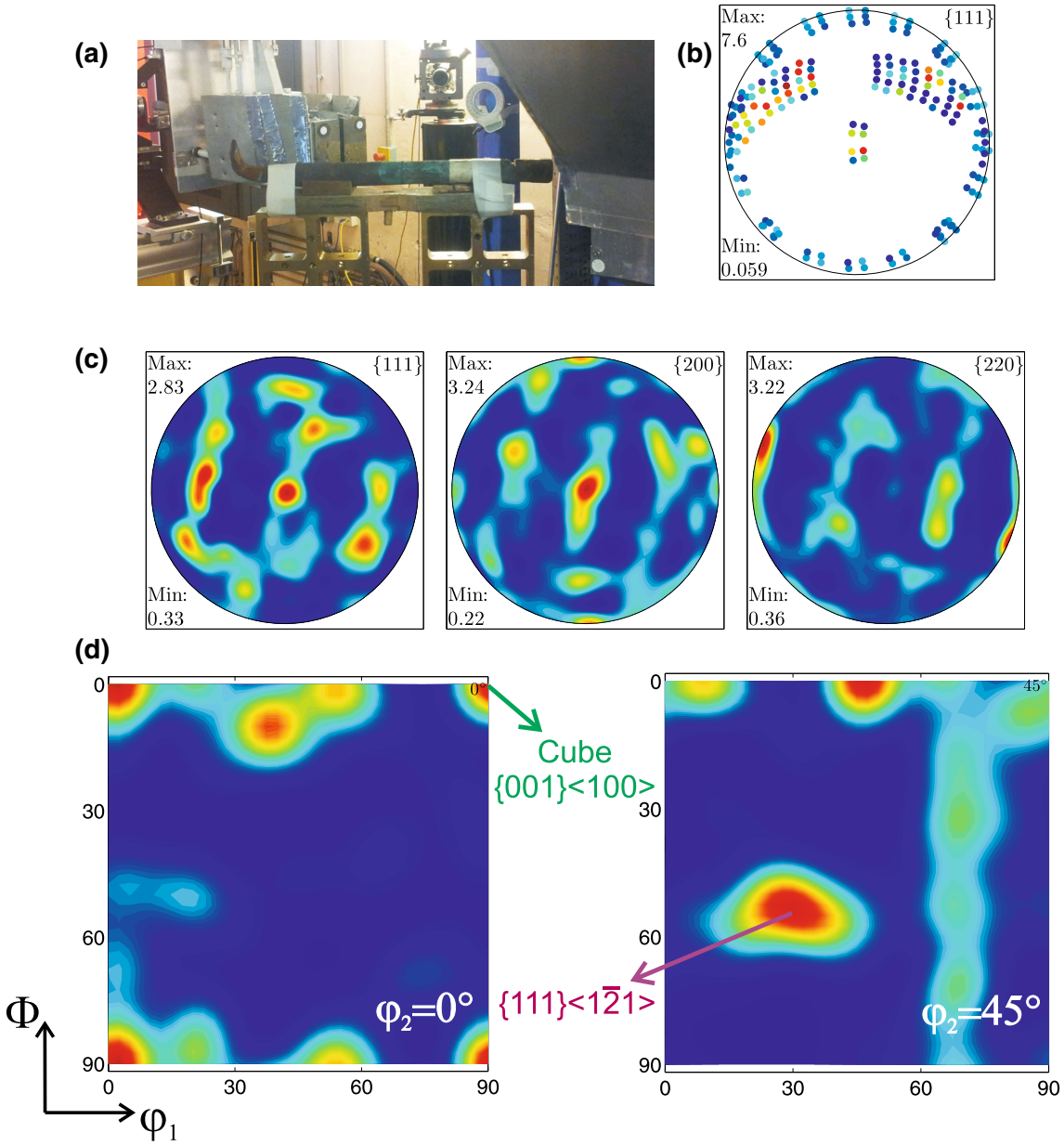

Fig. 6 **a** Photograph of the AB1-02-01 sample in ENGIN-X. **b** The experimental pole figure showing the angular coverage achieved by the measurement. **c** Recalculated pole figures from the ODF, calculated with MTEX from experimental pole figures such as (**b**). **d** Cuts of the ODF at $\varphi_2 = 0°$ and $\varphi_2 = 45°$, showing the main texture components of the material

methodologies in defining the copper bolt texture and demonstrate that the pole figure coverage achieved by the implemented neutron methodology fully described the principal texture components.

6.1.2 AB1-02-01 sample

The AB1-02-01 sample (Fig. 6a) was measured on ENGIN-X using an instrument configuration and data analysis strategy identical to that for the segment specimen (gauge volume of $4 \times 4 \times 4$ mm^3, incident beam divergence of $\approx 0.7° \times 0.8°$ (horizontal $\times$ vertical) and virtual detectors in 2×5 gridding scheme). TOF diffractograms were collected at 10 specimen orientations with counting times of ~ 12 min per orientation. This strategy yielded a total of 200 points for each experimental pole figure, as shown in Fig. 6b for the {111} pole figure. Again, the ODF of the material was calculated with MTEX from the {111}, {200}, {220} and {311} experimental pole figures assuming triclinic sample symmetry. Figure 6c shows recalculated pole figures and Fig. 6d two sections of the ODF ($\varphi_2 = 0°$ and $\varphi_2 = 45°$). The two main texture

Table 1 Volume fractions of the principal texture components of the segment sample, obtained by the different texture analysis measurements

	Neutron diffraction (%)	EBSD measurements (%)	X-ray diffraction (%)
⟨111⟩-fibre	40	45	38
⟨100⟩-fibre	12.5	8	14

components emerge from the plots; there are a $\{111\}\langle 1\bar{2}1\rangle$ component, with a volume fraction of 14 % of the crystallites, and a $\{001\}\langle 100\rangle$ cube component, due to recrystallization, with a 15.5 % volume fraction. The volume fractions were computed by MTEX using a 20° radius sphere centred at each orientation.

6.2 HMS impregnable

6.2.1 Forbes bolt

Neutron texture measurements were taken in the complete bolt from the HMS Impregnable, using the same methodology and experimental configuration as for the HSM Pomone samples. TOF diffractograms were collected at 10 specimen orientations with counting times of ~12 min per orientation, and the data were analysed using a 2×5 gridding scheme. This strategy yielded a total of 200 points for each experimental pole figure. However, due to the Forbes bolt's large diameter, the path lengths for some virtual detectors generates extremely low absorption correction factors for some reflections (as is shown in Fig. 3b), which reduces the number of the useful virtual detectors. In this case, only 162 detectors were used in the {111} pole figure (Fig. 7b), 170 in the {200}, 182 in the {220} and 185 in the {311} experimental pole figures. The ODF was calculated with MTEX from those experimental pole figures assuming triclinic sample symmetry. Figure 7c shows recalculated pole figures and Fig. 7d three sections of the ODF ($\varphi_2 = 0°$, $\varphi_2 = 45°$ and $\varphi_2 = 65°$). The main texture components present in the ODF section plots are listed in Table 2, which their corresponding Euler angles (using the Bunge convention) and volumes fractions, computed by MTEX using a 20° radius sphere centred at each orientation.

The $\{001\}\langle 100\rangle$ component and the $\{122\}\langle 212\rangle$ component are typical cube and twin cube components resulting from recrystallization during thermal annealing of rolled metals. Their presence is taken as evidence of thermal treatment after mechanical working, as the orientated recrystallization cannot take place without previous rotation of the crystallites due to plastic deformation [2]. However, the presence of the $\{111\}\langle 2\bar{3}1\rangle$ and the $\{111\}\langle \bar{1}\,\bar{1}2\rangle$ components demonstrate that the sample is not completely annealed, since it preserves the texture features related to mechanical working in the bolt axis direction.

7 Discussion and conclusions

In this work, we have employed a new texture analysis methodology using ENGIN-X, a TOF neutron strain scanner, to perform texture analyses on three copper bolts from two identified wrecks, *HMS Pomone* and *HMS Impregnable*. The method is based on splitting ENGIN-X detection banks into a number of smaller virtual detectors of sharper angular resolution and defining the ODF of the material from a number of incomplete experimental pole figures using the MTEX Toolbox. Since the pole figure coverage is strictly dependent on the range of orientations explored by the experiment and the gridding scheme employed to analyse the data, here we validated the present method and the measurement strategy by complementary experiments on the segment sample using EBSD measurements and laboratory X-ray diffraction. The excellent agreement shown by the three methodologies in defining the copper bolt texture (Table 1) demonstrates that the pole figure coverage achieved by the implemented neutron methodology fully described the principal texture components of the sample. In all cases, the recalculated pole figures (Figs. 4c, 5a, c) for the segment show a marked double fibre texture, with a strong γ-fibre and a minor ⟨100⟩ fibre component, typical of axisymmetrically drawn and annealed products made of fcc metals with medium or high stacking fault energies. The EBSD orientation image taken in the centre of a cross section through the bolt segment (Fig. 5b) confirms the grain structure to be fully recrystallized, presenting moderate levels of deformation in the recrystallized grains.

The complete specimen from the *HMS Pomone* presents a similar behaviour to the segment sample, with ⟨111⟩ and ⟨100⟩ type components parallel to the bolt axis direction. In this case, the crystallites are not iso-orientated around the {111} and the {100} crystal planes, and therefore, the recalculated pole figures (Fig. 6c) do not show a double fibre texture as in the segment sample. The two main texture components of the complete bolt are displayed in Fig. 6d. The presence of the $\{111\}\langle 1\bar{2}1\rangle$ texture component indicates a good alignment of the 111 planes parallel to the bolt axis, which is a feature commonly associated with extensional deformation along the symmetry axes of fcc metallic wires [2]. On the other hand, the development of a high symmetry component as the $\{001\}\langle 100\rangle$ cube

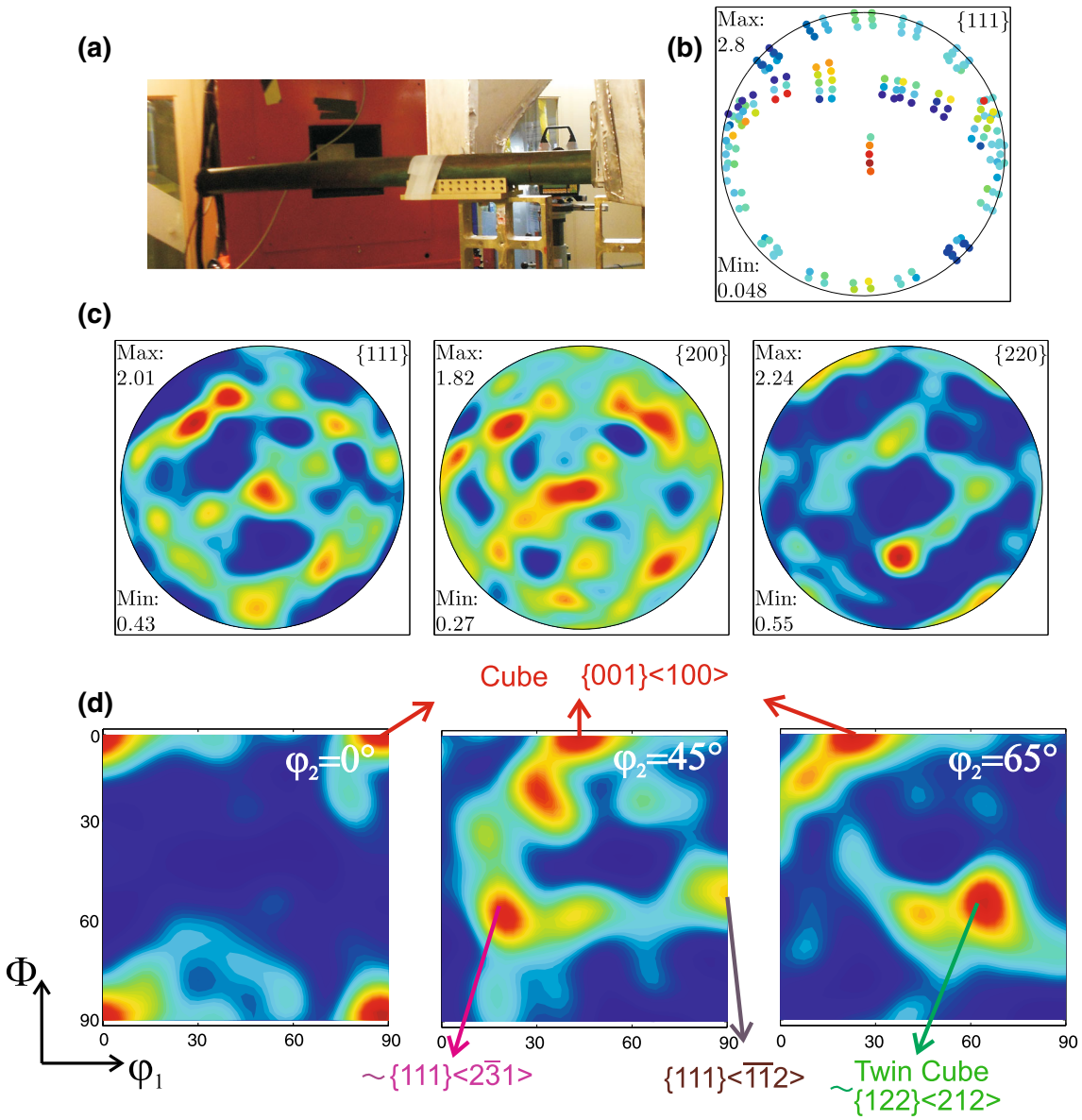

Fig. 7 **a** Photograph of the Forbes bolt sample in ENGIN-X. **b** The experimental pole figure showing the angular coverage achieved by the measurement. **c** Recalculated pole figures from the ODF calculated with MTEX from experimental pole figures. **d** Cuts of the ODF at $\varphi_2 = 0°$, $\varphi_2 = 45°$ and $\varphi_2 = 65°$, showing the main texture components of the material

Table 2 Principal texture component obtained for the Forbes bolt sample

	Euler angles (Bunge convention)			Volume fraction (%)
	φ_1 (°)	Φ (°)	φ_2 (°)	
{001}⟨100⟩	0	0	0	7.2
{122}⟨212⟩	63	48	63	7.6
{111}⟨2$\bar{3}$1⟩	20	55	45	7.6
{111}⟨$\bar{1}\,\bar{1}$2⟩	90	55	45	7.2

component is a direct manifestation of the sample recrystallization. However, the similar volumes obtained for both components reveal the complete bolt to be only partially recrystallized.

The recalculated pole figures (Fig. 7c) obtained for the complete bolt from the HMS Impregnable display a weaker texture than the other bolts, with maximum pole densities at about 2.4 mrd and minimum densities of 0.2 mrd. The

absence of a considerable texture might seem to indicate that the bolt has neither been strongly worked nor extensively heat treated [1]. However, the copper is known to have been reduced from a billet to a bar and then reduced to its present size either by grooved rolls or through a swage [4, 5]. The presence of the $\{001\}\langle 100\rangle$ and the $\{122\}\langle 212\rangle$ components reveals a thermal treatment after mechanical working, as the orientated recrystallization cannot take place without previous rotation of the crystallites due to plastic deformation [2]. On the other hand, the presence of the $\{111\}\langle 2\bar{3}1\rangle$ and $\{111\}\langle \bar{1}\,\bar{1}2\rangle$ components demonstrates that the sample is not completely annealed, since it preserved the texture features related to mechanical working in the bolt axis direction.

In the present state of research in copper sheathing and fastenings for wooden warships, the outstanding questions for archaeologists are processed, how the bolts were produced and supplied, performance, how they behaved in service, and preservation, everything that has happened to the bolts since the ship came to rest on the seabed. Neutron diffraction experiments in a TOF neutron strain scanner can give non-destructive quantitative texture analysis with spatial resolution. Since the crystallographic texture is critically dependent on the mechanical and thermal histories of the material, texture analysis provides important information relating to the manufacture and deformation history of the sample. This paper has successfully demonstrated the value of this new strategy in addressing the first question by differentiating between different production processes for different types of bolts without the need for unacceptably intrusive sampling. On the basis of the present results, the small diameter bolts were drawn, while the large bolts were rolled and swaged. The next step is to map texture across the diameters of bolts since, for example, documented cold hardening of the surface of the bolt can be expected to produce a signal, as could the driving of the bolt into the hull and its subsequent mechanical history in a continually flexing hull. This stage in the research is now being prepared for publication.

References

1. R. Arletti, L. Cartechini, R. Rinaldi, S. Giovannini, W. Kockelmann, A. Cardarelli, Appl. Phys. A **90**, 9–14 (2008)
2. G. Artioli, Appl. Phys. Mater. Sci. Process. **89**, 899–908 (2007)
3. J.-H. Cho, A.D. Rollett, J.S. Cho, Y.J. Park, J.T. Moon, K.H. Oh, Metall. Mater. Trans. A Phys. Metall. Mater. Sci. **37**, 3085 (2006)
4. D. Forbes, Letters from David Forbes to William Forbes, October–December 1783, Falkirk Archives A727.1766 (1783)
5. W. Forbes, *Ships' Bolts and Fastenings*, UK Patent Specification, No. 1381 (1783)
6. R. Hielscher, H. Schaeben, J. Appl. Crystallogr. **41**, 1024–1037 (2008)
7. J.A. James, J.R. Santisteban, L. Edwards, M.R. Daymond, Phys. B Condens. Matter **350**, 743–746 (2004)
8. F. Kropff, J.R. Granada, R.E. Mayer, Nucl. Instrum. Methods Phys. Res. **198**, 515–521 (1982)
9. F. Malamud, J.R. Santisteban, V. Alvarez, R. Bolmaro, J. Kelleher, S. Kabra, W. Kockelmann, J. Appl. Crystallogr. **47**, 1337–1354 (2014)
10. H. Park, D.N. Lee, Metall. Mater. Trans. A **34A**, 531–541 (2003)
11. V. Randle, *Microtexture determination and its applications*, 2nd edn. (Maney Publishing, UK, 2013)
12. J. Santisteban, L. Edwards, M. Fitzpatrick, A. Steuwer, P. Withers, M. Daymond, M. Johnson, N. Rhodes, E. Schooneveld, Nucl. Instrum. Methods Phys. Res. Sect. Accel. Spectrom. Detect. Assoc. Equip. **481**, 765–768 (2002)
13. J.R. Santisteban, M.R. Daymond, J.A. James, L. Edwards, J. Appl. Crystallogr. **39**, 812–825 (2006)
14. S. Siano, L. Bartoli, W. Kockelmann, M. Zoppi, M. Miccio, Phys. B Condens. Matter **350**, 123–126 (2004)
15. S. Siano, L. Bartoli, J.R. Santisteban, W. Kockelmann, M.R. Daymond, M. Miccio, G. De Marinis, Archaeometry **48**, 77–96 (2006)
16. R. van Langh, L. Bartoli, J. Santisteban, D. Visser, J. Anal. At. Spectrom. **26**, 892–898 (2011)
17. D.-Q. Wang, J.R. Santisteban, L. Edwards, Nucl. Instrum. Methods Phys. Res. Sect. Accel. Spectrom. Detect. Assoc. Equip. **460**, 381–390 (2001)